Synchrobetatron-coupling effects in alternating-phase-focusing linacs

Wen-Hao Cheng, Robert L. Gluckstern, and Hiromi Okamoto*
Physics Department, University of Maryland, College Park, Maryland 20742
(Received 4 August 1993)

Simultaneous longitudinal and transverse focusing can be obtained in a drift tube linac by alternating the sign of the synchronous phase. It is found both theoretically and numerically that, in the alternating-phase-focused (APF) linac with a symmetric synchronous phase sequence, the lowest-order resonance due to the synchrobetatron coupling naturally occurs, causing significant emittance transfer between the longitudinal and transverse motions. Equations for the averaged APF motion are derived to investigate the coupling effect. Two approximate invariants are obtained. Results from computer simulations based on a modified PARMILA code yield good agreement with the formulas for the invariant and tune shift derived from the theory. We then suggest a way to move the parameters away from the lowest-order resonance. Simulation results for the effect of space charge on the emittance exchange along with the synchrobetatron coupling are briefly discussed.

PACS number(s): 41.85.−p, 41.75.Ak

I. INTRODUCTION

It is well known that longitudinal stability can be obtained in a drift tube linac (DTL) by traversing each gap as the rf accelerating field rises. However, the rising accelerating field leads to a transverse defocusing force which is usually overcome by the use of magnetic focusing elements inside the drift tubes. The development of the radio-frequency quadrupole (RFQ) linac, which is now widely used in the energy region below around 3 MeV, is one way to provide for simultaneous longitudinal and transverse focusing without the use of focusing magnets.

With the advent of strong focusing, it was recognized that one could avoid the use of magnets by traversing alternately the region between adjacent drift tubes as the field is rising and falling, thus providing an alternation of focusing and defocusing forces in both the longitudinal and transverse directions [1, 2]. Explorations of this idea [3–5] show that the stable longitudinal phase space area is smaller than for the Alvarez type DTL. However, it is not clear that the parameter space has been explored fully, and recent efforts suggest that alternating phase focusing (APF) may permit low-velocity acceleration of currents in the 100–300 mA range [6]. Compared to an RFQ or a usual DTL with magnets, an APF structure is clearly simpler and therefore much cheaper. The absence of the focusing elements inside the drift tubes enables us to use an APF linac in the energy region below a few MeV at sufficiently high operating frequency.

While superconducting RFQ has recently been of interest [7, 8], it is much easier to design a superconducting version of the APF linac because of its simple structure. Making an APF linac superconducting is also beam-dynamically beneficial because it permits very high gradient operation which is always required for an APF design to make the acceptances sufficiently large. Additionally, in the usual DTL case, high field gradient produces the strong rf-defocusing force at each gap, which may deteriorate the beam quality. But in the APF case, we do not have to worry about this kind of effect because the gap defocusing fields are essential to achieve the strong focusing. Moreover, the application of modified APF structures to ion implantation technology has also been considered lately [9]. In Russia, there actually exist several APF machines intended mainly for heavy-ion acceleration [10, 11], and APF beam dynamics has been extensively studied [12–14].

In an earlier paper [15], we tested the predictions obtained in an analytical study of the current carrying capacity of an APF linac [16] by adapting the simulation code PARMILA [17] to the APF structure. We found, however, that significant emittance growth arose even in a low intensity beam for which phase-space matching was approximately achieved. In the present paper, we show that the emittance growth for a matched beam without space charge is a response to the lowest-order resonance which naturally occurs in symmetric APF [18]. In Sec. II, coupled equations of motion for APF without space charge are derived using a Fourier series method. A smoothed version of the coupled equations is given in Sec. III, leading to the condition for the lowest-order resonance. In Sec. IV, the coupled system is simplified by the Krylov-Bogoliubov-Mitropolsky (KBM) averaging method [19, 20]. We also consider the effect of the nonlinear longitudinal oscillation which causes an amplitude dependent tune shift, and results of analysis and simulation are presented. Two invariants are derived and discussed in Sec. V, and solutions of the reduced coupled equations of motion are briefly discussed, for both the constant β case and with acceleration. In Sec. VI, we show how to move the parameters away from the resonance and provide confirming evidence from particle simulations. Finally, space-charge effects are also included in the simulations, and a brief description of the results

*Permanent address: Accelerator Laboratory, Institute for Chemical Research, Kyoto University, Gokanoshou, Uji, Kyoto 611, Japan.

is given in Sec. VII.

In the following study, we assume the synchronous phase alternation pattern

$$\phi_{s(i)} = -\phi_0 - \phi_1, \quad i = 1, 2, \ldots, N/2$$

$$\phi_{s(i)} = -\phi_0 + \phi_1, \quad i = N/2 + 1, \ldots, N$$

where N is an even integer corresponding to the number of gaps in a single focusing period of length $N\beta_s\lambda$ ($\equiv L_N$). Here, both ϕ_0 and ϕ_1 are positive, with ϕ_0 representing a small asymmetric offset to accompany the large alternating ϕ_1. The desired synchronous phase configuration can be obtained by choosing drift tube lengths that alternate appropriately. It is, of course, possible to choose a negative value for ϕ_0. However, we will only use positive values of ϕ_0 in order to meet the large acceptance requirement [5].

II. COUPLED EQUATIONS OF MOTION

For an APF structure, one can obtain the corresponding equations of motion by a Fourier expansion of the step functions [5]. If we assume that the fractional change of $\beta_s\gamma_s$ is small over a focusing period and introduce τ_i, the dimensionless coordinate of the ith gap center position divided by L_N in a focusing period, as

$$\tau_i(i \neq 1) = \frac{1}{N}\sum_{n=1}^{i-1} \frac{2\pi + \phi_{s(n+1)} - \phi_{s(n)}}{2\pi} \text{ with } \tau_1 = 0,$$

the transverse and longitudinal equations of motion for a 2π-mode APF structure are found to be

$$\frac{d^2x}{d\tau^2} + \frac{NK}{k_w} I_1(k_w x) \sum_{i=1}^{N} \Lambda_i(\tau) \sin(\psi + \phi_{s(i)}) = 0, \tag{2.1}$$

$$\frac{d^2\psi}{d\tau^2} + NK \sum_{i=1}^{N} \Lambda_i(\tau)[I_0(k_w x)\cos(\psi + \phi_{s(i)}) - \cos\phi_{s(i)}] = 0, \tag{2.2}$$

where I_0 and I_1 are the modified Bessel functions, ψ is the particle phase relative to the synchronous phase ϕ_s, $\tau \equiv s/L_N$, $k_w \equiv 2\pi/\beta_s\gamma_s\lambda$, and

$$\Lambda_i(\tau) = 1 + 2\sum_{n=1}^{\infty} S_{ni}\cos[2n\pi(\tau - \tau_i)].$$

Here $S_{ni} \equiv \sin(n\pi g_i/L_N)/(n\pi g_i/L_N)$, where g_i is the ith gap length in a focusing period. Since $g_i \ll L_N$, we simply put $S_{ni} \approx 1$ in the analysis. In Eqs. (2.1) and (2.2), K is a dimensionless parameter defined by

$$K \equiv \frac{2\pi e q E_0 T \lambda}{m_0 c^2 \beta_s \gamma_s^3},$$

where q is the charge state of an accelerated ion and E_0T is the effective average accelerating field. While K is, in general, a function of τ, we keep it constant along the structure by ramping the accelerating field as $\beta_s\gamma_s^3$, fixing also the values of ϕ_0, ϕ_1, and N. This procedure is required, as concluded in the previous work [15], to achieve simultaneous beam matching in both directions while keeping the phase acceptance and transverse beam size constant across any transition [21,22].

To study the coupled motion governed by Eqs. (2.1) and (2.2), the higher-order powers in x and ψ, as well as the linear term, must be taken into account. In the following analysis, we consider the terms containing $O(x^2)$ and $O(x\psi)$, which cause the synchrobetatron coupling, and the terms $O(\psi^2)$ and $O(\psi^3)$, which yield the longitudinal amplitude dependent tune shift. Then, Eqs. (2.1) and (2.2) yield

$$x'' + K_s(\tau)x = -K_c(\tau)x\psi, \tag{2.3}$$

$$\psi'' - 2K_s(\tau)\psi = K_c(\tau)\left(\psi^2 - \frac{k_w^2}{2}x^2\right) - \frac{K_s(\tau)}{3}\psi^3, \tag{2.4}$$

where the prime indicates $d/d\tau$ and

$$K_s(\tau) = B_s + \sum_{n=1}^{\infty} C_{s(n)}\sin(2n\pi\tau + \theta_{s(n)}), \tag{2.5}$$

$$K_c(\tau) = B_c + \sum_{n=1}^{\infty} C_{c(n)}\sin(2n\pi\tau + \theta_{c(n)}). \tag{2.6}$$

The Fourier coefficients in Eqs. (2.5) and (2.6), which are all real, are given by

$$B_c + jB_s = \frac{KN}{2}\sum_{i=1}^{N} e^{j\phi_{s(n)}}, \tag{2.7}$$

$$C_{s(n)}e^{j\theta_{s(n)}} = KN\sum_{i=1}^{N} e^{j2n\pi\tau_i}\sin\phi_{s(i)}, \tag{2.8}$$

$$C_{c(n)}e^{j\theta_{c(n)}} = KN\sum_{i=1}^{N} e^{j2n\pi\tau_i}\cos\phi_{s(i)}. \tag{2.9}$$

Note that since the coupling terms in Eqs. (2.3) and (2.4) involve ψ and k_w, and the longitudinal oscillation amplitude ψ is adiabatically damped as β_s increases, the synchrobetatron coupling motion decreases as beam energy increases.

III. RESONANCE

Before proceeding further to describe the synchrobetatron resonance, let us derive the smoothed version of the coupled equations of motion. We first decompose the solutions for x and ψ into a slowly varying part and a high frequency part as

$$x(\tau) = \chi(\tau) + \sum_{n=1}^{\infty} a_n(\tau)\sin(2n\pi\tau + \theta_{s(n)}),$$

$$\psi(\tau) = \varphi(\tau) + \sum_{n=1}^{\infty} b_n(\tau)\sin(2n\pi\tau + \theta_{s(n)}),$$

where $\chi(\tau)$, $\varphi(\tau)$, $a_n(\tau)$, and $b_n(\tau)$ are slowly varying functions. Substituting them into Eqs. (2.3) and (2.4), the coefficients of the high-frequency terms give the approximate solutions

$$a_n(\tau) \approx \frac{C_{s(n)}}{(2n\pi)^2}\chi(\tau), \quad b_n(\tau) \approx -\frac{2C_{s(n)}}{(2n\pi)^2}\varphi(\tau). \tag{3.1}$$

By averaging out the rapidly varying part and using Eq. (3.1), we then obtain the smoothed equations of motion as follows:

$$\chi'' + \sigma_t^2\chi = -\sigma_a^2\chi\varphi, \tag{3.2}$$

$$\varphi'' + \sigma_\ell^2\varphi = \sigma_b^2\varphi^2 + \sigma_d^2\varphi^3 - \frac{k_w^2}{2}\sigma_c^2\chi^2, \tag{3.3}$$

where writing

$$P_n \equiv \frac{C_{s(n)}^2}{(2n\pi)^2}\ , \quad P = \sum_{n=1}^{\infty} P_n\ , \quad S = \sum_{n=1}^{\infty}\frac{P_n}{(2n\pi)^2}\ ,$$

$$T = \sum_{n=1}^{\infty}\frac{P_n^2}{(2n\pi)^2}\ , \quad Q_n \equiv \frac{C_{s(n)}C_{c(n)}}{(2n\pi)^2}\ , \quad Q = \sum_{n=1}^{\infty} Q_n\ ,$$

the coefficients in Eqs. (3.2) and (3.3) can be represented as

$$\sigma_t^2 = B_s + P/2\ , \quad \sigma_\ell^2 = -2B_s + 2P, \tag{3.4}$$

$$\sigma_a^2 = B_c(1-S) - Q/2\ , \quad \sigma_b^2 = B_c(1+2S) - 2Q, \tag{3.5}$$

$$\sigma_c^2 = B_c(1+S/2) + Q\ , \quad \sigma_d^2 = -B_s/3 + P - 2S - T. \tag{3.6}$$

To illustrate the occurrence of the synchrobetatron coupling resonance, we ignore the nonlinear longitudinal oscillation terms and concentrate, at this stage, only on the coupling terms $\sigma_a^2\chi\varphi$ and $k_w^2\sigma_c^2\chi^2/2$. The second-order solutions of Eqs. (3.2) and (3.3) without the $O(\psi^2)$ and $O(\psi^3)$ terms are

$$\begin{aligned}\chi_{(2)}(\tau) = {} & \chi_1\cos(\sigma_t\tau + \delta_t) \\ & -\frac{\sigma_a^2}{4\sigma_t}\chi_1\varphi_1\left[\left(\frac{1}{\Delta_+} - \frac{1}{\sigma_\ell}\right)\cos(\sigma_+\tau + \delta_+)\right. \\ & \left. + \left(\frac{1}{\Delta_-} + \frac{1}{\sigma_\ell}\right)\cos(\sigma_-\tau + \delta_-)\right],\end{aligned} \tag{3.7}$$

$$\begin{aligned}\varphi_{(2)}(\tau) = {} & \varphi_1\cos(\sigma_\ell\tau + \delta_\ell) \\ & -\left(\frac{k_w\chi_1\sigma_c}{2\sigma_\ell}\right)^2\left[1 - \frac{\sigma_\ell^2}{\Delta_+\Delta_-}\cos 2(\sigma_t\tau + \delta_t)\right],\end{aligned} \tag{3.8}$$

where

$$\Delta_\pm = 2\sigma_t \pm \sigma_\ell,$$

$$\sigma_\pm = \sigma_t \pm \sigma_\ell,$$

$$\delta_\pm = \delta_t \pm \delta_\ell,$$

and χ_1, φ_1, δ_t, and δ_ℓ are determined by the initial values of $\chi_{(2)}$ and $\varphi_{(2)}$. From Eq. (3.4), we can see that $\Delta_- = 0$ when $B_s = 0$, which corresponds to the case of $\phi_0 = 0$ because of Eq. (2.7). That is, the lowest-order resonance occurs whenever a symmetric phase sequence is chosen for the APF linac. Other higher-order resonances can also exist when taking the higher-order coupling terms into account. However, the (2,1) difference resonance described above is the lowest order and the most severe one, as long as there is no troublesome sum resonance. Thus, to avoid the rapid growth of oscillation amplitudes or a large emittance exchange between the transverse and longitudinal motions, a nonzero phase offset ϕ_0 should be employed. More correctly speaking, phase alternation patterns with nonzero values of B_s should be chosen for a practical APF design. As described later, we can restrict the emittance growth due to the coupling, even if the system is exactly on resonance. A detailed discussion to avoid the coupling resonance is given in Sec. VI.

IV. KRYLOV-BOGOLIUBOV-MITROPOLSKY AVERAGING

Upon treating the coupling and nonlinear oscillation terms on the right-hand sides of Eqs. (3.2) and (3.3) as the forcing terms that drive the linear oscillations close to resonance, we may try to find solutions of these equations similar to the solutions of the linear system, but with slowly varying amplitudes and phases. Specifically, we write

$$\chi(\tau) = X(\tau)\cos[\sigma_t\tau + \alpha(\tau)], \tag{4.1}$$

$$\varphi(\tau) = \Phi(\tau)\cos[\sigma_\ell\tau + \beta(\tau)], \tag{4.2}$$

with the conditions

$$\chi'(\tau) = -\sigma_t X(\tau)\sin[\sigma_t\tau + \alpha(\tau)], \tag{4.3}$$

$$\varphi'(\tau) = -\sigma_\ell\Phi(\tau)\sin[\sigma_\ell\tau + \beta(\tau)]. \tag{4.4}$$

The first-order derivatives of $X(\tau), \Phi(\tau), \alpha(\tau)$, and $\beta(\tau)$ can be obtained by substituting Eqs. (4.1) and (4.2) into Eqs. (3.2) and (3.3), using Eqs. (4.3) and (4.4). Then, the rates of change of the phase and amplitude functions in both directions can be approximated by taking their averages over one cycle of rapid variation, according to the well-known KBM method. The high-frequency modes are averaged out and only the low-frequency Δ_- parts near or on resonance are kept. Straightforward algebra yields the averaged version of the equations as

$$X'(\tau) = \frac{\sigma_a^2}{4\sigma_t}X(\tau)\Phi(\tau)\sin\Psi(\tau), \tag{4.5}$$

$$\Phi'(\tau) = -\frac{k_w^2\sigma_c^2}{8\sigma_\ell}X^2(\tau)\sin\Psi(\tau), \tag{4.6}$$

$$\alpha'(\tau) = \frac{\sigma_a^2}{4\sigma_t}\Phi(\tau)\cos\Psi(\tau), \tag{4.7}$$

$$\beta'(\tau) = \frac{k_w^2}{8}\frac{\sigma_c^2}{\sigma_\ell}\frac{X^2(\tau)}{\Phi(\tau)}\cos\Psi(\tau) - \nu_1\Phi^2(\tau), \tag{4.8}$$

where

$$\Psi(\tau) = \Delta_-\tau + 2\alpha(\tau) - \beta(\tau) \tag{4.9}$$

and

$$\nu_1 = \frac{3\sigma_d^2}{8\sigma_\ell}. \tag{4.10}$$

It is also an easy matter to estimate the amplitude dependence of the tune shift in the longitudinal motion. For this purpose, we again apply Eqs. (4.1) and (4.2) together with Eqs. (4.3) and (4.4) to Eq. (3.3), neglecting the coupling term χ^2. Expanding the amplitude and phase in a perturbation series, we can easily show, in the second-order approximation, that

$$\langle\beta'(\tau)\rangle \approx -(\nu_1+\nu_2)\Phi_0^2(\tau), \tag{4.11}$$

where $\Phi_0(\tau)$ is the zeroth-order term in the perturbation expansion of $\Phi(\tau)$, $\langle\beta'(\tau)\rangle$ denotes the averaged value of $\beta'(\tau)$, and

$$\nu_2 = \frac{5\sigma_b^4}{12\sigma_\ell^3}. \tag{4.12}$$

The longitudinal oscillation frequency is hence detuned by the following expression:

$$\omega_\ell = \frac{d}{d\tau}\theta_\ell(\tau) = \sigma_\ell + \langle\beta'(\tau)\rangle \approx \sigma_\ell - \Delta\omega_\ell\Phi_0^2, \tag{4.13}$$

where

$$\Delta\omega_\ell = \nu_1+\nu_2 = \frac{3\sigma_d^2}{8\sigma_\ell} + \frac{5\sigma_b^4}{12\sigma_\ell^3}. \tag{4.14}$$

In Fig. 1, we compare the results of the analytical approximation in Eq. (4.14) with the single particle simulations by PARMILA modified for APF structure, and the agreement is good in spite of using only the lowest-order approximation.

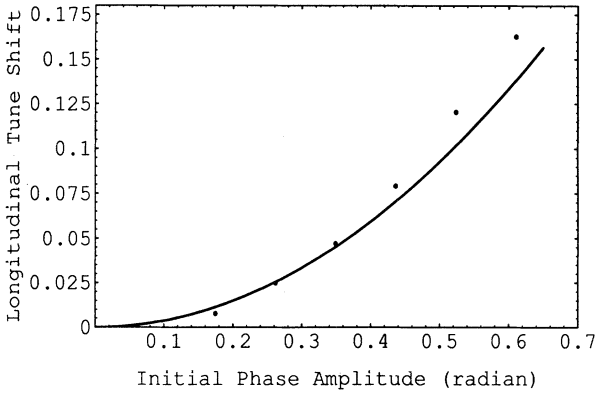

FIG. 1. Longitudinal tune shift $\Delta\omega_\ell$ with respect to the initial phase amplitude Φ_0. The dots are the results of a single particle simulation and the solid line shows the analytical result from Eq. (4.14). The parameters are $K = 0.556$, $N = 4$, $\phi_1 = 70°$, and $\phi_0 = 0$.

V. INVARIANTS OF THE COUPLED MOTION

A. Amplitudes and first invariant

From Eqs. (4.5) and (4.6), we see that there exists the invariant

$$\frac{\sigma_t}{\sigma_a^2}X^2(\tau) + 2\frac{\sigma_\ell}{k_w^2\sigma_c^2}\Phi^2(\tau) = E_1 = \text{ const.} \tag{5.1}$$

This first invariant can be easily related to $\chi(\tau)$ and $\varphi(\tau)$ in Eqs. (4.1) and (4.2), which indicate that $\chi_{\max}\chi'_{\max} = \sigma_t X^2(\tau)$ and $\varphi_{\max}\varphi'_{\max} = \sigma_\ell\Phi^2(\tau)$. Assuming the uniform particle distributions both longitudinally and transversely, the averaged maximum amplitudes $X(\tau)$ and $\Phi(\tau)$ can be written as

$$X^2(\tau) = \frac{\epsilon_x}{\sigma_t}\left(\frac{N\lambda}{\gamma}\right), \quad \Phi^2(\tau) = \frac{\epsilon_\psi}{\sigma_\ell}\left(\frac{k_w^2}{2\pi}\frac{N\lambda^2}{\gamma}\right), \tag{5.2}$$

where ϵ_x and ϵ_ψ are the normalized effective emittances, respectively, in the transverse $x - p_x$ and longitudinal $\psi - \Delta W$ phase space. Here, the effective emittance has been defined as four times the rms emittance. The first invariant E_1 is now rewritten as

$$E_1 = \frac{N\lambda}{\gamma}\left[\frac{\epsilon_x}{\sigma_a^2} + 2\frac{\epsilon_\psi}{\sigma_c^2}\left(\frac{\lambda}{2\pi}\right)\right]. \tag{5.3}$$

From the expressions in Eqs. (3.5) and (3.6) it can be seen that σ_a^2 and σ_c^2 are close to each other due to the fact that their difference consists of terms of order K^2 and K^3. In addition, we also observe that the form of E_1 is not very sensitive to acceleration. If we rewrite $\epsilon_\psi\lambda/2\pi$ as ϵ_z and neglect the higher-order corrections, the first invariant is then simply

$$E_1 \approx \frac{N\lambda}{B_c}(\epsilon_x + 2\epsilon_z). \tag{5.4}$$

The accuracy of the first invariant in Eq. (5.3) has been checked by using PARMILA. The simulation results in Fig. 2 show the transfer of normalized rms emittance between the longitudinal and transverse motions, confirming the validity of Eq. (5.3). Many simulations with different parameters have also been obtained, all confirming the validity of the formula for E_1 as an approximate invariant.

Note that the existence of the first invariant enables us to reduce the two differential equations for the amplitudes, Eqs. (4.5) and (4.6), into one differential equation with the help of a new function

$$J(\tau) = \frac{2\sigma_\ell\Phi^2(\tau)}{\sigma_c^2k_w^2E_1} \approx \frac{2N\lambda\epsilon_z}{\sigma_c^2E_1}, \tag{5.5}$$

which implies that

$$1 - J(\tau) = \frac{\sigma_t X^2(\tau)}{\sigma_a^2E_1} \approx \frac{N\lambda\epsilon_x}{\sigma_a^2E_1}. \tag{5.6}$$

The differential equation for $J(\tau)$ is therefore

$$J'(\tau) = -\eta_1[1 - J(\tau)]\sqrt{J(\tau)}\sin\Psi(\tau), \tag{5.7}$$

where

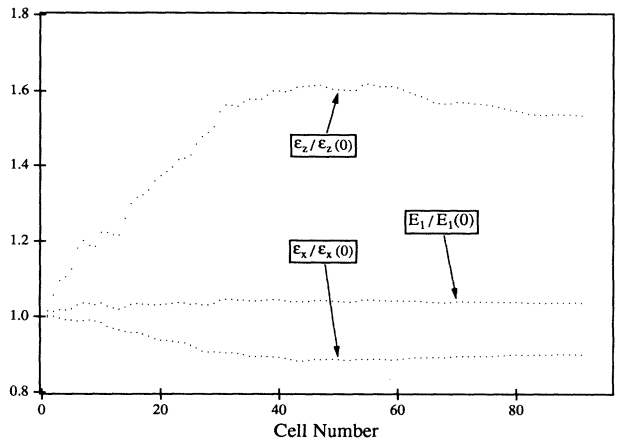

FIG. 2. Simulation results for the emittance transfer between the longitudinal and transverse motion and the first invariant from Eq. (5.3). The initial emittances are $\epsilon_x = 0.5242$ cm mrad and $\epsilon_z = 0.0758$ cm mrad. The parameters are the same as those used in Fig. 1.

$$\eta_1 = \frac{\sigma_a^2 k_w}{2\sigma_t}\sqrt{\frac{\sigma_c^2 E_1}{2\sigma_\ell}}. \tag{5.8}$$

B. Coupling phase and second invariant

While the equations for the amplitudes give the first invariant, the equations for the phases, Eqs. (4.7) and (4.8), can also be integrated in a similar way to give the coupling phase in terms of the varying amplitude [22]. Differentiating Eq. (4.9) and using Eqs. (4.7) and (4.8) with the definition given by Eqs. (5.5) and (5.6), we have

$$\Psi'(\tau) = \Delta_- + \eta_2\nu_1 J(\tau) + \eta_1\left(\frac{3J(\tau)-1}{2\sqrt{J(\tau)}}\right)\cos\Psi(\tau), \tag{5.9}$$

where

$$\eta_2 = \frac{k_w^2\sigma_c^2 E_1}{2\sigma_\ell} = \left(\frac{2\sigma_t}{\sigma_a^2}\right)^2\eta_1^2. \tag{5.10}$$

Dividing Eq. (5.9) by Eq. (5.7), we get a formula for an exact differential as follows:

$$d[\sqrt{J}(1-J)\cos\Psi] = \frac{1}{\eta_1}(\Delta_- + \eta_2\nu_1 J)dJ. \tag{5.11}$$

Let us now temporarily ignore the damping of k_w due to the increase of β_s, which causes the decreases of the parameters η_1 and η_2. With the ansatz of constant β_s, we can then integrate Eq. (5.11) treating the parameters η_1 and η_2 as constant. The coupling phase is then given by

$$\cos\Psi(\tau) = \frac{-E_2 + \left[\Delta_- + \frac{\eta_2}{2}\nu_1 J(\tau)\right]J(\tau)}{\eta_1[1-J(\tau)]\sqrt{J(\tau)}}, \tag{5.12}$$

where the second invariant E_2 is the constant of integration and can be determined from the initial conditions of the variables J and Ψ at the injection point of a linac.

A plot of $\cos\Psi$ as a function of J, in the manner of Sturrock's phase-amplitude diagram [23], gives a qualitative description of the behavior of the system. Figure 3 shows an example of the phase-amplitude diagram for Eq. (5.12) with the same parameters as in Fig. 2. The stable zone of the diagram shown is within the region $-1 \le \cos\Psi \le 1$ and $0 \le J \le 1$. As we can see from Fig. 3, a coherent emittance oscillation takes place for any initial points $J(0)$ and $\Psi(0)$ on the phase-amplitude diagram. The rise or fall of an emittance at the beginning depends upon the initial amplitude $J(0)$, i.e., the ratio of the longitudinal emittance to the sum of the emittances. If the initial J starts near the left margin of the phase-amplitude diagram, the longitudinal emittance will tend to grow while the transverse emittance decreases. If one starts the initial J close to the right margin of the phase-amplitude diagram, the situation is then just reversed. In either case, the first invariant is always conserved along the channel.

C. Analytic solution for constant β

Analytical solutions for J and Ψ can, in fact, be obtained by solving Eqs. (5.7) and (5.9) under the ansatz of constant β_s. From Eqs. (5.7) and (5.12), we get

$$J' = -G(J), \tag{5.13}$$

where

$$G(J) = \sqrt{\sum_{i=1}^{4} c_i J^i}, \tag{5.14}$$

and

$$c_0 = -E_2^2, \quad c_1 = \eta_1^2 + 2E_2,$$

$$c_2 = -2\eta_1^2 + E_2\eta_2\nu_1 - \Delta_-^2,$$

$$c_3 = \eta_1^2 - \Delta_-\eta_2\nu_1, \quad c_4 = -(\eta_2\nu_1/2)^2.$$

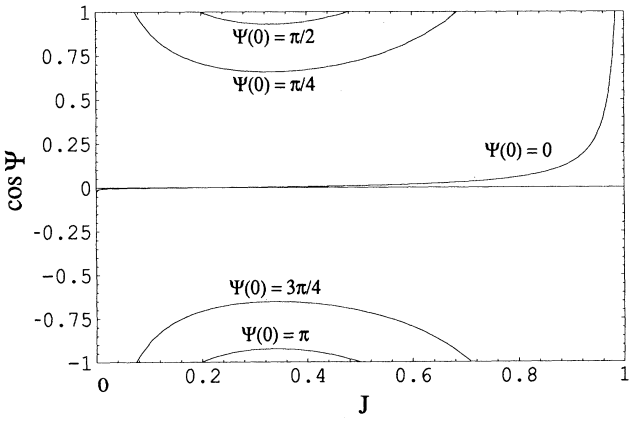

FIG. 3. Phase-amplitude diagram. The parameters are the same as those used as Fig. 2.

We can then solve τ in terms of J as

$$-\tau = \int_{J(0)}^{J} \frac{dJ}{G(J)} = gF(\xi|m) - gF(\xi_0|m), \qquad (5.15)$$

where $F(\xi|m)$ is the elliptic integral of the first kind, $\xi_0 = \xi(J=0)$,

$$\xi(J) = \sin^{-1}\sqrt{(a-c)(J-b)/(a-b)(J-c)},$$

$$m = (a-b)(c-d)/(a-c)(b-d),$$

$$g = 2/\sqrt{(a-c)(b-d)},$$

and we have defined the roots of $G(J)$ as a, b, c, d and $a > J > b > c > d$. The solution for $J(\tau)$ is

$$J(\tau) = \frac{c\alpha^2 \mathrm{sn}^2\left(\frac{(\tau_0-\tau)}{g}\middle|m\right) - b}{\alpha^2 \mathrm{sn}^2\left(\frac{(\tau_0-\tau)}{g}\middle|m\right) - 1}, \qquad (5.16)$$

where $\mathrm{sn}(x|m)$ is the Jacobian elliptic function, $\tau_0 = gF(\phi_0|m)$, and $\alpha^2 = (a-b)/(a-c)$.

The τ-dependent trajectories of $J(\tau)$ and $\Psi(\tau)$ must lie on the curves in Fig. 3, which oscillate rapidly in J between 0 and 1. An example of the behavior of $J/J(0)$ with the same parameters as in Fig. 3 is shown in Fig. 4. It is seen that the emittance exchange due to coupling causes a prompt emittance oscillation.

D. Results for constant acceleration

When we include the acceleration effect associated with synchrobetatron coupling, it is clear that Eq. (5.3) still holds even if the parameter changes due to acceleration are taken into account. However, the solution of constant β in Eq. (5.16) is no longer valid because the parameters η_1 and η_2 now depend on τ. As an example, let us assume the particle's velocity β_s changes as

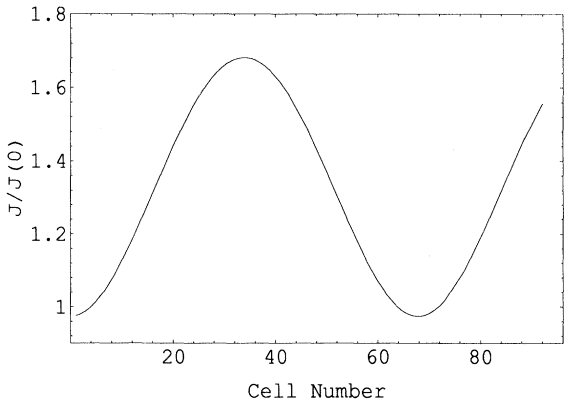

FIG. 4. The emittance oscillation under the assumption of constant velocity. The parameters are the same as those used in Fig. 2.

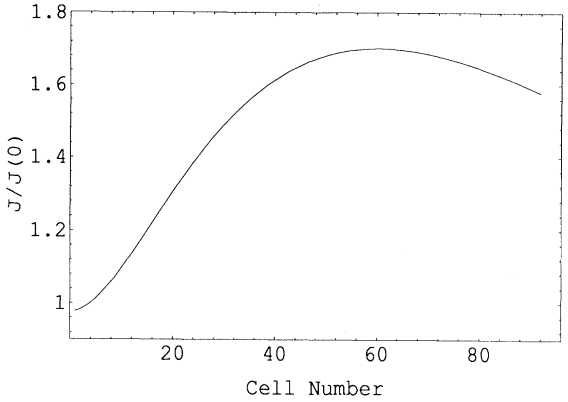

FIG. 5. The behavior of emittance growth under the assumption of constant acceleration. The parameters are the same as those used in Fig. 2.

$$\frac{\beta_s(\tau)}{\beta_s(0)} \approx 1 + \left(\frac{KN}{2\pi}\cos\phi_1\right)\tau, \qquad (5.17)$$

approximating the parameters $\eta_1(\tau)$ and $\eta_2(\tau)$ correspondingly. In this case, the forms of Eqs. (5.7) and (5.9) remain the same except that $\eta_1(\tau)$ and $\eta_2(\tau)$ are now τ dependent, and we can find the approximate solutions for $J(\tau)$ and $\Psi(\tau)$ which involve both the sine and cosine integrals. Figure 5 shows the behavior of $J(\tau)/J(0)$ found by numerical integration for the case of constant acceleration. The parameters and initial emittances are the same as those used in Fig. 2. Comparing the numerical integration result of Fig. 5 and the PARMILA simulation in Fig. 2, we observe that their behaviors are quite similar qualitatively, except for different growth rates and saturation ranges. Furthermore, we can also conclude that the saturation of emittance exchange, i.e., decoupling of the coupled oscillation, is due to the effect of acceleration which reduces the coupling strengths.

VI. AWAY FROM RESONANCE

It is worthwhile to note that the result of Eqs. (5.7) and (5.9) can also be derived from the Hamiltonian, treating $J(\tau)$ and $\Psi(\tau)$ as the action-angle variables. The Hamiltonian in this case is just identical to the second invariant:

$$H(\Psi, J) = E_2 = \Delta_- J + \frac{\eta_2}{2}\nu_1 J^2 - \eta_1(1-J)\sqrt{J}\cos\Psi. \qquad (6.1)$$

The phase space of the Hamiltonian flow for the system (6.1) on resonance is plotted in Fig. 6. The two fixed points on the resonance manifold can be found via the conditions: $J' = 0$ and $\Psi' = 0$, where $\Psi = 0$ (in phase) and π (out of phase). Noting that the values of η_1 and η_2 are usually smaller than 1, and $\eta_2\nu_1 \ll \eta_1$ (e.g., $\eta_1 \approx 0.368$ and $\eta_2\nu_2 \approx 0.0129$ in the example of Fig. 2), we can neglect the $\eta_2\nu_1$ term in Eq. (5.9). The fixed points of the system on resonance are then approximately equal to

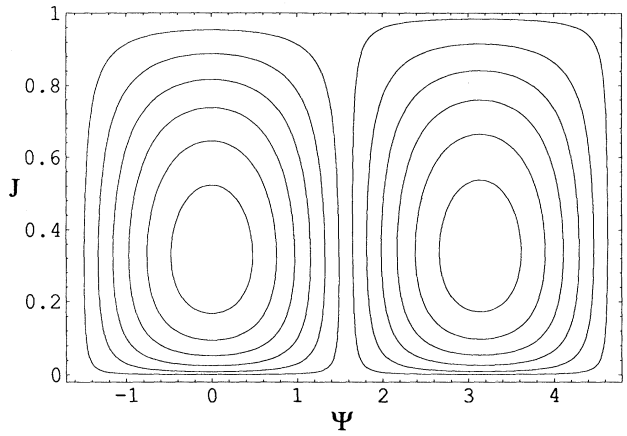

FIG. 6. Phase space of the resonance manifold.

$$J \approx \frac{1}{3}, \quad \Psi = 0, \pi, \tag{6.2}$$

where the amplitude dependent tune-shift term modifies the value of J at the fixed points only slightly. According to Eqs. (5.3) and (5.5), we can see that when

$$J = 1/3,$$

the ratio of longitudinal and transverse emittances has the following relationship:

$$\frac{\epsilon_z}{\epsilon_x} = \frac{1}{4}\left(\frac{\sigma_c}{\sigma_a}\right)^2 \approx \frac{1}{4}. \tag{6.3}$$

If we inject a beam having the emittance ratio ϵ_z/ϵ_x near 1/4 into an APF linac with the zero phase offset, then the particles in the beam that are nearly in phase ($\Psi = 0$) and the particles that are nearly out of phase ($\Psi = \pi$) will oscillate within only a small range of J around the fixed points. If the emittance ratio is exactly equal to 1/4, the in-phase and out-of-phase particles will remain in an approximately stationary state. The particles with other phases will follow the Hamiltonian flow on the resonance manifold. Their amplitudes will either decrease or increase, depending on their initial locations in phase space.

Note that in Fig. 6, the phase space is plotted for constant β. Although acceleration could cause the parameters in the Hamiltonian to decrease adiabatically, the trajectories with acceleration in fact still follow a pattern in phase space similar to the case without acceleration. And the fixed points for the resonance manifold are almost unchanged even if η_1 and η_2 are damping along the structure. Therefore, if the beam has an initial emittance J smaller than 1/3, particles following the Hamiltonian flow will distribute through the whole phase space. Meanwhile, the quasiperiodic motions around the fixed points are also slowing down due to acceleration. Consequently, the overall average of J will grow and saturate. For an initial J larger than 1/3, the average behavior of J decreases and then saturates. On the other hand, for a beam with initial J near 1/3, the variation

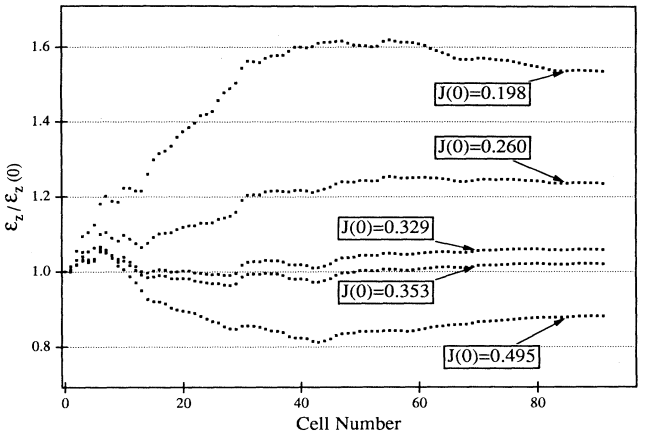

FIG. 7. Simulation results for the longitudinal emittance growth of different initial scaled emittance J, where the system is on resonance. The parameters are the same as those used in Fig. 2.

of J on average will almost remain the same as the initial J. Simulations of the bunched beam for different scaled emittance ratios, shown in Fig. 7, confirm this prediction. Note that the results shown in Figs. 4 and 5 are obtained by numerical integration of Eqs. (5.7) and (5.9) with the initial condition $J_0 = 0.198$. In Fig. 4, J oscillates around the fixed point which is near 1/3 as expected, with the difference involving the amplitude dependent tune shift.

As mentioned in Sec. III, to avoid the coupling resonance, we should use a nonzero phase offset ϕ_0 in the phase pattern as defined in Sec. I. The nonzero detuning Δ_- will cause the Hamiltonian flow to change in the phase space. The fixed points of the off-resonance manifold can be found from the stationary solution of Eq. (5.9) when $\Psi' = 0, \Psi = 0$ or π, and the $\eta_2\nu_1$ term is ignored. Here we define a quantity

$$R \equiv \left|\frac{\Delta_-}{\eta_1}\right| - \left|\left(\frac{3J-1}{2\sqrt{J}}\right)\right|, \tag{6.4}$$

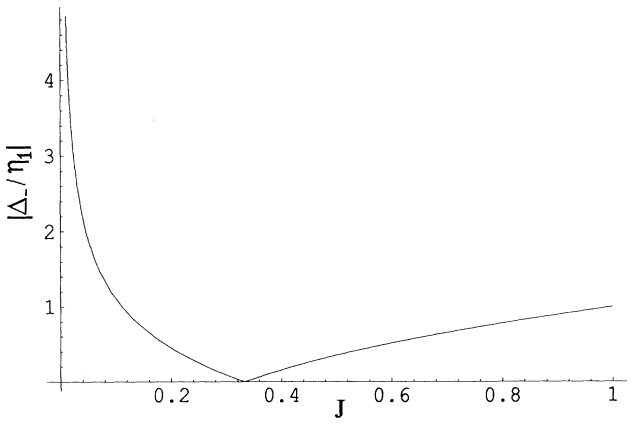

FIG. 8. The scaled resonance band vs the scaled longitudinal emittance. The curve is where $R = 0$.

which measures the value of the scaled detuning $|\Delta_-/\eta_1|$ away from the fixed points. When R is near zero, the coupled system operates near the fixed points and thus a smaller emittance exchange is expected. The plot of the fixed-point line is shown in Fig. 8. The fixed point of the on-resonance manifold, $J \sim 1/3$, clearly corresponds to the intersection of the curve with the J axis.

Results of PARMILA simulations for $\epsilon_z(\tau)/\epsilon_z(0)$ [i.e., $J(\tau)/J(0)$] are shown in Fig. 9. Since the first invariant holds for any parameters along the channel, here we examine only one of the emittances. We show three cases of different values of J. In Figs. 9(a) and 9(c), the initial J's are located at the left-hand side and the right-hand side of the zero detuning fixed point $J \sim 1/3$, which correspond to a short bunch and a long bunch, respectively. Figure 9(b) illustrates the behaviors of the longitudinal emittance of the coupled system when J is near $1/3$. It is observed that smaller values $|R|$ give smaller emittance exchange.

Let us now recapitulate the main results of Secs. V and VI. We here conclude that, by the KBM averaging method, two invariants are obtained and the analytical and numerical solutions of the averaged coupled system show that the saturation of emittance exchange is due to the decoupling caused by acceleration. While the first invariant enables us to reduce the system of two degrees of freedom to one degree of freedom, the second invariant, which is equivalent to the transformed Hamiltonian of the coupled system, gives us the fixed point. When the synchrobetatron coupling is on resonance, using a matched beam with emittance ratio $\epsilon_z/\epsilon_x \approx 1/4$ such that $J \approx 1/3$ will give an almost-stationary beam, where the emittance growth is much smaller than the beam with other initial values of J. If the coupling is off resonance, the system still needs to be adjusted, for a specific value of J, such that the quantity R defined in Eq. (6.4) is close to zero, i.e., the beam must be introduced close to the fixed point of the Hamiltonian system. To sum up, the best operating points of an APF system, as far as the synchrobetatron coupling effect is concerned, are located along the curve of Fig. 8.

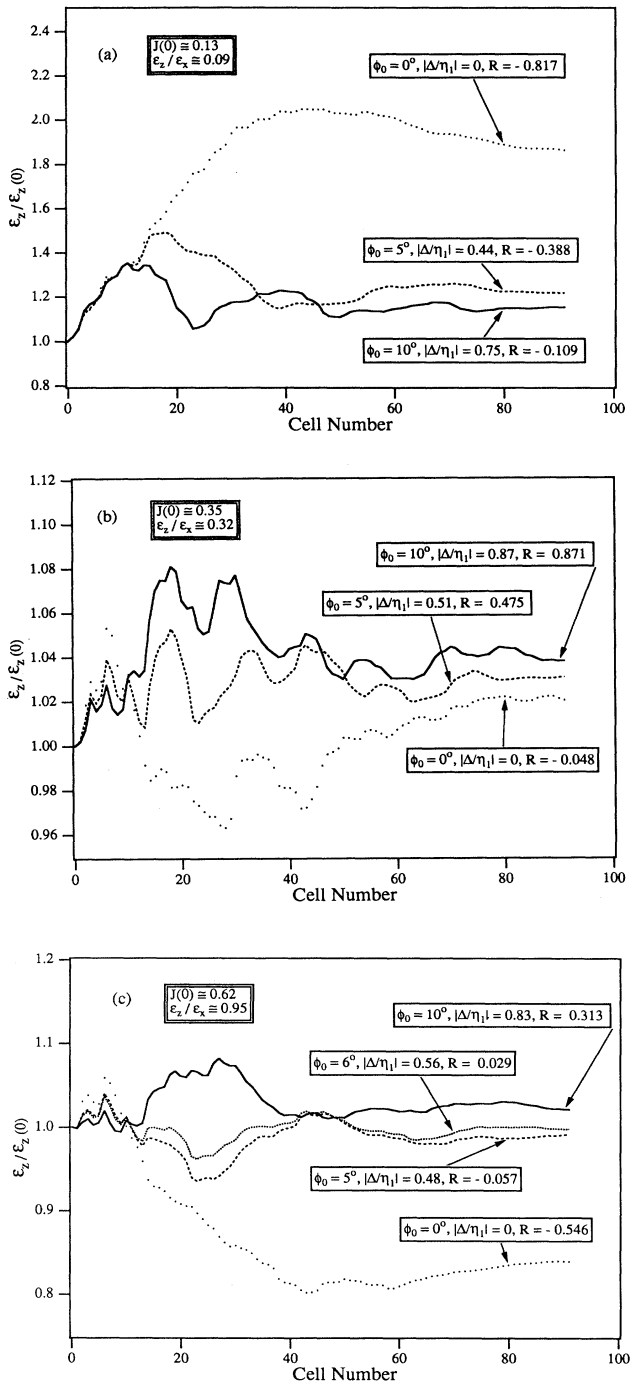

FIG. 9. Simulation results for the emittance growth with different phase offsets. The parameters are $K = 0.556$, $N = 4$, and $\phi_1 = 70°$. (a) Initial $J(0) = 0.13$, which corresponds to a short bunch; (b) $J(0) = 0.35$, near the on-resonance fixed point; (c) $J(0) = 0.62$, corresponding to a longer bunch, compared with the previous cases.

VII. SPACE-CHARGE EFFECT

In this section, we present simulation results including space charge. By using the same parameter set we

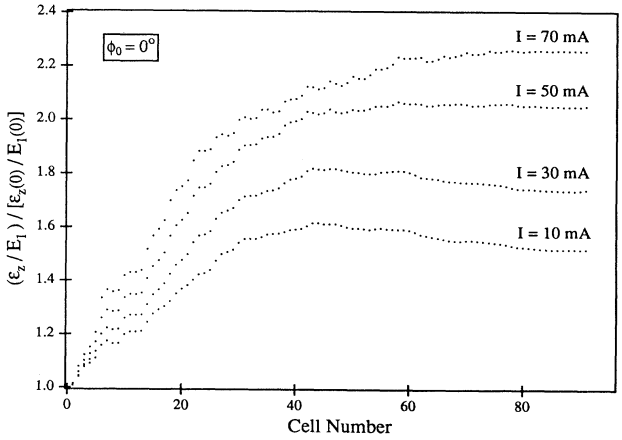

FIG. 10. Simulation results for the emittance growth with different currents. The parameters are $K = 0.556$, $N = 4$, $\phi_1 = 70°$, and $\phi_0 = 0$.

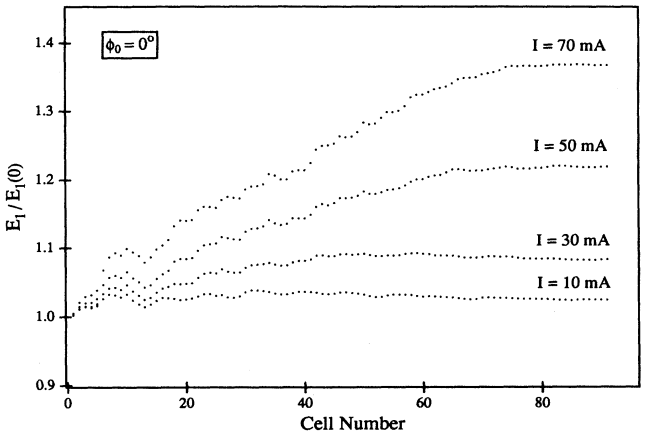

FIG. 11. Simulation results for E_1 with different currents. The parameters are $K = 0.556$, $N = 4$, $\phi_1 = 70°$, and $\phi_0 = 0$.

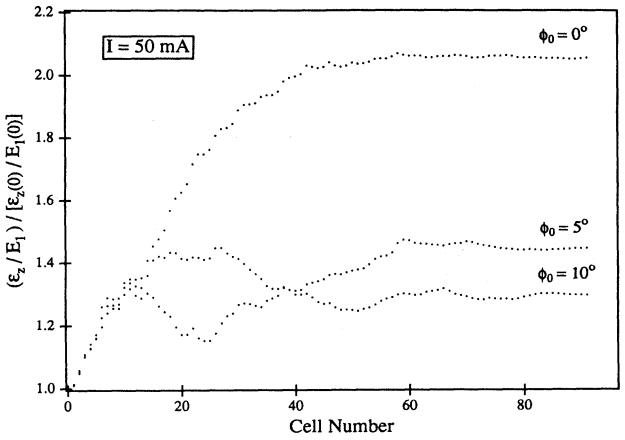

FIG. 12. Simulation results for the emittance growth with different phase offsets. The parameters are $K = 0.556$, $N = 4$, and $\phi_1 = 70°$.

used in the previous examples, we find that space charge enhances the rate and range of the emittance exchange. As expected, the emittance growth rate increases with increasing beam intensity (see Fig. 10). Space charge also induces a substantial growth in E_1 as shown in Fig. 11, and E_1 is no longer an invariant. This growth of E_1 is reasonable, because the higher-order nonlinear terms due to space charge neglected in Eqs. (2.3) and (2.4) are expected to make greater contributions to the beam behavior as the intensity increases. On the other hand, as shown in Fig. 12, a nonzero phase offset can still move the operating point away from resonance even if there is space charge.

VIII. SUMMARY

The equations of coupled motion for an APF linac have been truncated, smoothed, and averaged. Numerical simulations confirm the theoretical predictions fairly well with regard to the longitudinal tune shift and the first invariant. We have shown, in both the simulations and the analysis, that the emittance exchange due to synchrobetatron coupling can be decreased, as shown in Sec. VI, by either choosing the optimum emittance ratio or by introducing a nonzero phase offset in the phase pattern of the APF linac. Specifically, the best operating point of APF system is where

$$|\Delta_-/\eta_1| \simeq |(3J-1)/2\sqrt{J}|.$$

We also included space charge in the simulations and found that the transfer of emittance due to both effects, i.e., synchrobetatron coupling and space charge effect, can still be reduced significantly by introducing a positive ϕ_0.

ACKNOWLEDGMENTS

W.H.C. and H.O. would like to thank Professor I. M. Kapchinsky for useful discussions and Professor A. J. Dragt for his valuable suggestions. Special thanks go to Dr. T. Wangler and S. Nath for their help in adapting the subroutine of PARMILA to the APF structure.

[1] M. L. Good, Phys. Rev. **92**, 538 (1953).
[2] Y. B. Faynberg, CERN Report No. CERN-91-100, 1956.
[3] D. A. Swenson, Part. Accel. **7**, 61 (1976).
[4] I. M. Kapchinsky, *Theory of Resonance Linear Accelerators* (Harwood Academic Publishers, New York, 1985).
[5] H. Okamoto, Nucl. Instrum. Methods A **284**, 233 (1989).
[6] N. Wells, *Radio Frequency Quadrupole and Alternating Phase Focusing Methods Used in Proton Linear Accelerator Technology in the USSR* (Rand Corporation, Santa Monica, 1985).
[7] I. Ben-Zvi, A. Lombardi, and P. Paul, Part. Accel. **35**, 177 (1991).
[8] J. R. Delayen *et al.*, Proc. IEEE Part. Accel. Conf. **4**, 2441 (1991).
[9] A. N. Antropov *et al.*, in *Proceedings of the European Particle Accelerator Conference, Rome, 1988*, edited by Sergio Tazzari (World Scientific, Singapore, 1988), Vol. 2, p. 1451.
[10] I. V. Chuvilo *et al.*, in *Proceedings of the European Particle Accelerator Conference, Rome, 1988*, edited by Sergio Tazzari (World Scientific, Singapore, 1988), Vol. 2, p. 1024.
[11] V. V. Kushin, N. A. Nesterov, I. O. Parahin, and S. V. Plotnikov, Proc. IEEE Part. Accel. Conf. (to be published).
[12] A. N. Antropov, V. K. Baev, N. M. Gavrilov, S. A. Minaev, and A. V. Shal'nov, Zh. Tekh. Fiz. **59**, 124 (1989) [Sov. Phys.—Tech. Phys. **34** (7), 786 (1989)].
[13] F. G. Garashchenko, V. V. Kushin, S. V. Plotnikov, L. S. Sokolov, I. V. Strashnov, P. A. Fedotov, I. I. Kharchenko, and A. V. Tsulaya, Zh. Tekh. Fiz. **52**, 460 (1982) [Sov. Phys.—Tech. Phys. **27** (3), 296 (1982)].
[14] L. Sagalovsky and J. R. Delayen, in *Proceedings of the 1992 Linear Accelerator Conference, Ottawa, 1992*,

edited by C. R. Hoffmann (AECL Research, Ottawa, 1992), Vol. 2, p. 763.

[15] W. H. Cheng, R. L. Gluckstern, S. Nath, and T. P. Wangler, in *Proceedings of the 1992 Linear Accelerator Conference, Ottawa, 1992*, edited by C. R. Hoffmann (AECL Research, Ottawa, 1992), Vol. 1, p. 193.

[16] R. L. Gluckstern and D. Vassiliadis, CEBAF Report No. CEBAF-89-001, 1989 (unpublished).

[17] G. Boicourt, *Proceedings of the Conference on Linear Accelerator and Beam Optics Codes, San Diego, CA*, edited by Charles R. Eminhizer, AIP Conf. Proc. No. 177 (AIP, New York, 1988).

[18] H. Okamoto, Bull. Inst. Chem. Res. Kyoto Univ. **69**, 1 (1991).

[19] N. N. Bogoliubov and Yu. A. Mitropolsky, *Asymptotic Methods in the Theory of Nonlinear Oscillations* (Gordon and Breach, New York, 1961).

[20] N. M. Krylov and N. N. Bogoliubov, *Introduction to Nonlinear Mechanics* (Princeton University Press, Princeton, 1947).

[21] Employing the E_0T-ramping scheme with a fixed phase sequence may result in unpracticable accelerating fields in higher energy parts of the structure. This situation could be overcome by making the value of N larger (see, for example, Ref. [5]).

[22] F. Verhulst, *Nonlinear Differential Equations and Dynamical Systems* (Springer-Verlag, Berlin, 1990).

[23] P. A. Sturrock, Ann. Phys. (N.Y.) **3**, 113 (1958).